Acta Microscópica, Vol. 1, Nº 1, May 1992, pp 29-42

Influence of Grain Size on the Corrosion Behaviour of a Commercial Aluminium - 1% Manganese Alloy

Mariana M . Staia , Eli S . Puchi and Rosa Vera
Escuela de IngenieríaMetalúrgica y Ciencia de los Materiales, Universidad Central de Venezuela, Apartado 49141, Zona Postal 1042-A, Caracas, Venezuela.

SUMMARY

The microstructural characterization of a number of samples of a commercial aluminium 1% manganese alloy subjected to a series of thermomechanical treatments and to standard corrosion tests, has been conducted by means of both light and electron microscopy techniques. The thermomechanical treatments carried out gave rise to a wide variety of grain sizes ranging between 24 to 320 μm, without a significant change in the shape, size and distribution of the secondary phase particles. The morphology of the corrosion products, when the applied potential was greater than the pitting potential was similar, independent of the grain size, to that of the alloy in the as-received condition and that corresponding to pure aluminium. EDX analysis of such products have shown that the ratios of Fe/Al and Cu/Al are higher within the corrosion pits than in the aluminum matrix. During the performance of general corrosion tests it has been observed that the thermomechanically treated samples displayed a greater corrosion resistance than samples of the material in the as-received condition, and that such a behaviour improves markedly as the grain size of the alloy decreases.

KEY WORDS

Grain size - aluminium alloy - general corrosion behavior - pitting.

* present address: Universidad Católica de Valparaiso, Avenida Brasil 2950, Casilla 4059, Valparaiso, Chile.

INTRODUCTION

The thermomechanical treatments applied to commercial aluminium alloys in order to develop specific mechanical properties can also influence directly the corrosion behaviour of the material. Such treatments give rise to many microstructural changes that range from changes in the grain structure to drastic alterations in the content and distribution of intermetallic particles, both of which can influence markedly the behavior of the alloy in a specific agressive medium. A number of investigations have been carried out in order to determine the effect of the metallurgical variables on the corrosion behaviour of the aluminium alloys [1-6].

Several authors [7,8] have reported that an inhomogeneous solute distribution within the aluminium matrix could give rise to the presence of areas with different values of pitting potential which would favor the selective attack of the material. In several cases [9], it has been observed a clear relationship between the volume fraction of second-phase particles and the number of pits formed on the surface of the alloy. Also, it has been shown that the chemical composition and particularly the ratio Mn/Fe in the aluminium-manganese alloys, could play a very important role in the corrosion resistance of the material [10-12]. However, there is not any information available in the current literature about the influence of the grain size on the corrosion behaviour of these particular alloys. Therefore the present investigation has been conducted in order to determine the influence of such a metallurgical variable on the corrosion resistance. This communication reports only the most important results concerning the microstructural characterization of the investigated material and its corrosion products, since other relevant results have been published elsewere [13].

EXPERIMENTAL PROCEDURE

1.- Thermomechanical treatment

The present study has been carried out with samples of a wrought commercial aluminium - 1% manganese alloy whose composition is given in Table 1.

Table I Chemical Analysis of the experimenta alloy, Wt %

Element	Mn	Si	Fe	Cu	Mg	Zn	Cr	Al
Wt%	0.925	0.230	0.645	0.140	0.006	0.004	0.004	balance

The material was supplied as plate of 4 mm thickness, in condition H14 (cold rolled and partially annealed). A number of samples were cut from the initial plate and annealed during 8 hours at a temperature of 550°C which allowed the development of a fully recristallized structure with a homogeneous grain size, from which both rolling and tensile specimens were machined. The rolling samples were deformed to an equivalent tensile strain of 2.33 (87% thickness reduction) whereas tensile specimens were deformed to effective strains of 0.11, 0.15 and 0.20 respectively. All the deformed specimens were subsecuently annealed in a salt bath at 550° ± 3 °C during 1 hour for the rolled specimens and 3 hours for the tensile samples. After annealing, all the specimens were water quenched and prepared for metallographic and microscopic analysis. Smaller samples taken from the previously deformed and annealed specimens were grounded with SiC papers of grades 400,500 and 600, and subsequently polished with alumina paste of 1 μm, degreased and dried in a hot air stream. The metallographic observation was carried out in an optical microscope with cross polarizers employing a sample previously anodized in a solution of HF and distilled water. The grain size, was measured using the mean linear intercept method [14] and reported as the mean value of at least 300 grains. In order to characterize the distribution of large second phase particles (≥ 1 μm), the samples were also analyzed by means of Scanning Electron Microscopy techniques with EDX facilities for semicuantitative chemical analysis. The distribution of small second phase particles (≤ 0.1 μm) were characterized by means of Transmission Electron Microscopy techniques to analyze thin foils of the treated samples. On the other hand, the corrosion behaviour of the specimens was evaluated by means of standard immersion tests and electrochemical tests, carried out on small samples previously prepared metallographically as described before.

2.- Immersion Tests

2.a - General Corrosion

General corrosion tests were conducted in a triple set of samples of dimensions 2.0 x 2.0 x 0.1 cm and 2.2 x 1.0 x 0.7 cm. A solution of NaCl 1 M of pH 1.5 was used as electrolyte. The test was carried out at ambient temperature and the exposure times were of 0.5, 1, 2, 3, 5, 7, 10 and 15 days. At the end of each test the samples were carefully washed in a solution according of the ASTM standard B137-45, cleaned, dried and weighted. In the present case the extent of corrosion was determined by weight loss.

2.b - Pitting Corrosion

In order to determine the susceptibility of the alloy to pitting corrosion, a test previously developed by Alcan International [15] was conducted using three sets of samples of 1.5 x 3.8 cm and 2.0 x 1.0 cm. The samples were submersed during one month in the test solution which presented a pH of 8 a temperature of 25 °C. The samples were previously etched in a solution of 80% vol. H_3PO_4, 15% CH_3COOH and 5% HNO_3 during 3 min. at a temperature of 98º ± 2 ºC. After the experiment the specimens were removed and treated with the ASTM B137-45 solution. In order to determine the depth of the pits formed on the surface of the samples, vertical cuts were made along different chosen pits, mounted and grounded

with SiC paper grade 600. Afterwards, the specimens thus prepared were analized by SEM techniques whereas the pits depth was determined with a micrometer coupled to an optical microscope.

3. Electrochemical tests

Potentiodynamic and potentiostatic tests were carried out in samples of the alloy both in the as-received condition and thermomechanically treated. The experiments were conducted with a solution of NaCl 3.5% purged with nitrogen, exposing a sample area of about 2 cm^2. The experimental setting employed has been described in detail elsewere [15].

EXPERIMENTAL RESULTS AND DISCUSSION

1.- Thermomechanical treatment

1.a - Grain size

Table II sumarizes the results concerning the relationship between the applied strain and the final recristallized grain size obtained for all the samples thermomechanically treated and employed in the corrosion experiments.

fully recristallized specimens is composed of a number of equiaxed grains which indicates that the previously deformed matrix has been totally replaced by a new strain free structure giving rise to a drastic reduction in the dislocation density of the material. Obviously, as the degree of strain applied increases the recristallized grain size decreases since the recristallization process is carried out by the activation of a larger number of nuclei induced by a higher internal stored energy associated to a higher degree of deformation. However, in the short transverse direction, in the sample with the highest degree of applied strain ($\varepsilon = 2.33$), the grains present an aspect ratio very near to unity indicating the high homogeneous deformation induced in the specimen. Nevertheless, as the strain applied decreases its distribution becomes less homogeneous and the activated nuclei are farther apart. Thus, the intermetallic particles play a more important role in restraining the recristallization fronts from growing in the transverse direction rather than in the rolling or longitudinal direction which leads to a resulting structure with an aspect ratio somehow greater than unity.

Table II Variation of the final recristallized grain size with the effective strain applied

ε	2.33	0.20	0.15	0.11
d (μm)	24±2	147±12	216±17	320±25

Optical micrographs presented in Figures 1 and 2 show the microstructure corresponding to the specimens with the smallest and largest recristallized grain size in the short transverse direction, whereas Fig. 3 presents the microstructure of the material in the as-received condition along the longitudinal direction. As it can be observed from this last micrograph the microstructure of the alloy is constituted by elongated grains in the rolling direction since the annealing step after cold working has not been sufficient to promote recristallization and the replacement of the deformed matrix by a new microstructure composed of strain free and equiaxed grains. Therefore, it represents a microstructure with a high internal stored energy mainly in the form of dislocations. On the contrary, the microstructure corresponding to the

1.b- Particle distribution

Scanning electron micrographs presented in Figures 4-6 show the distribution of large second phase particles present in the alloy in the as-received condition and thermomechanically treated to produce the smallest and largest values of the final recristallized grain size respectively. Thus, it can be observed that independently of the thermomechanical treatment applied a low density of large particles (1-10μm) homogeneously distributed embbeded in the matrix is present. However, there are also present a large number of smaller particles ($\leq$ 1 μm) uniformily distributed, within the aluminium matrix. Large particles have different sizes and snapes ranging from spherical to elongated and irregular. The size of spherical

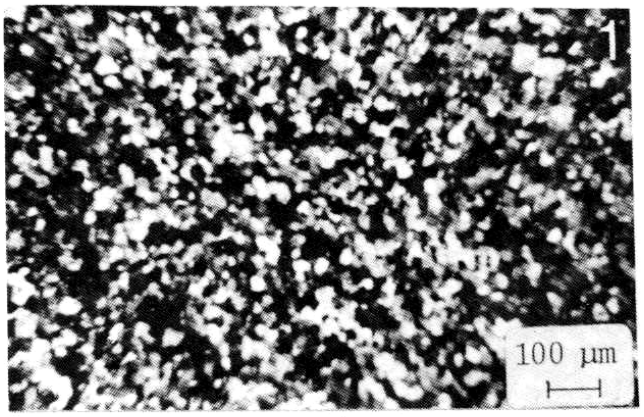

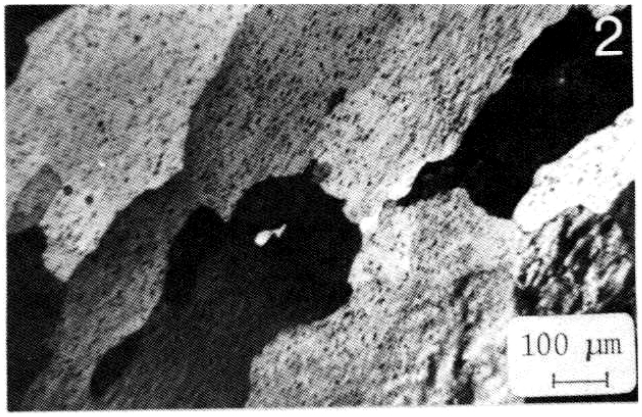

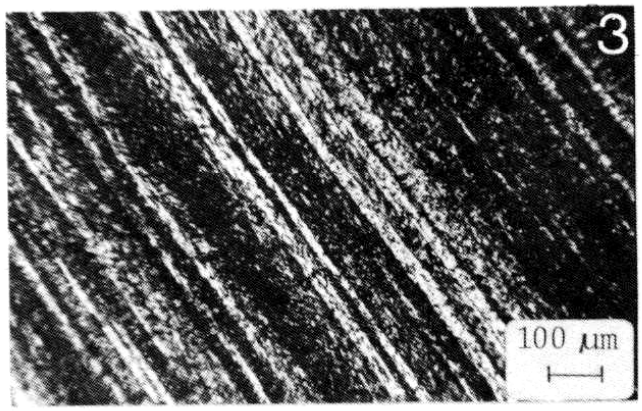

Fig. 1. Optical micrograph showing the grain structure of the alloy thermomechanically treated to produce a recrystallized grain size of 320µm. Polarized light.
Fig. 2. Optical micrograph showing the grain structure of the alloy thermomechanically treated to produce a recrystallized grain size of 24µm. Polarized light.
Fig. 3. Optical micrograph showing the grain structure of the alloy in the as-received condition. Polarized light.

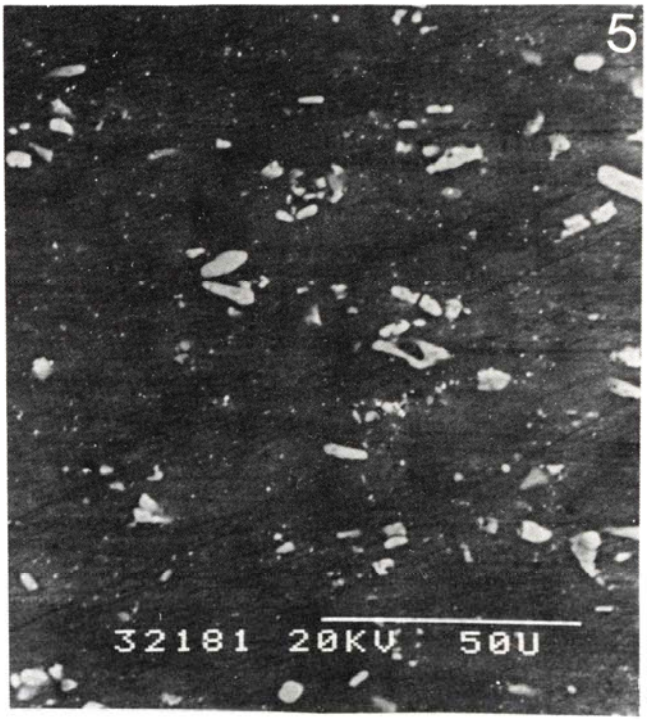

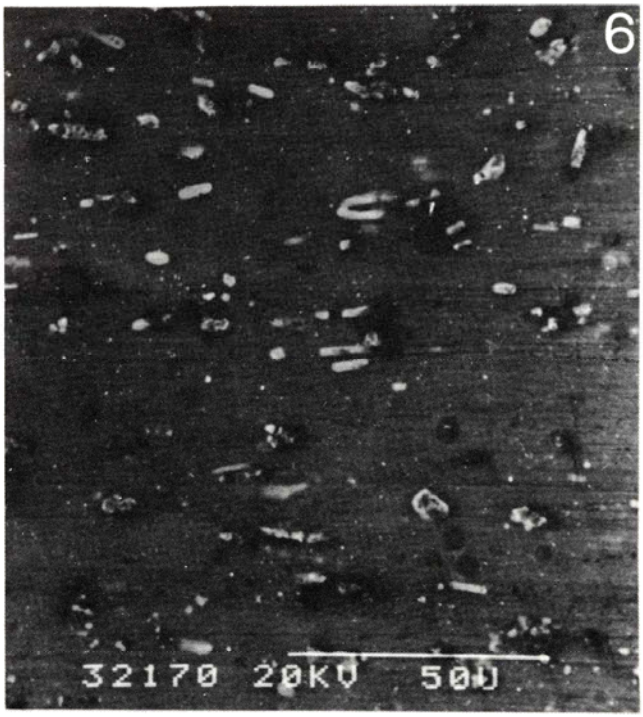

Fig. 4. Scanning micrograph showing the distribution of second-phase particles present in the as-received alloy.
Fig. 5. Scanning electron micrograph showing the distribution of second-phase particles present in the 320μm grain size alloy.
Fig. 6. Scanning electron micrograph showing the distribution of second-phase particles present in the 24μm grain size alloy.

particles varies between aproximately 4-5 μm whereas elongated particles can achieve up to 10 μm in length. Table III summarizes some relevant information concerning the number of particle per unit area and the volume fraction of large particles in relation to the condition of the alloy for the transversal and longitudinal orientation.

Table III Number of particles per unit area (N°) and particle volume fraction (fv) as a function of alloy condition and orientation

ε_{eq}	d(μm)	orientation	N°/mm^2	fv x 10^{-2}
2.33	24	L	3160	2.7
		T	3832	2.4
0.20	147	L	3392	3.6
		T	3096	2.9
0.15	216	L	3496	3.3
		T	3040	3.2
0.11	320	L	2944	3.6
		T	2560	3.3
as-recived material		L	3456	3.9
		T	2280	3.7

The mean value of the volume fraction has been found to be approximately 3.3x 10^{-2} independentely of the condition of the alloy, which agrees with typical values previously reported [16]. However, it can also be appreciated a slight increase in the number of particles per unit area as the strain applied increases which suggests that the smallest grain size is related to a larger number of intermetallic particles. The semicuantitative analysis of such particles showed that independently of their shape the composition is quite similar. Such intermetallic compounds are mainly constituted of Mn, Fe, Cu, Si and Cr and could be represented as $MnAl_3$, (Mn, Fe) Al_6, $FeAl_3$, $CuAl_2$ and α- Si (Mn, Fe)Al. The ratio Mn/Fe was found to be higher in the matrix than in the particles for the specimens thermomechanically treated, contrary to the observation made in the material in the as-received condition. Also, it has been observed a slight increase in the copper content in the matrix and in the particles as the grain size increases, whereas in the as-received condition the concentration of this element remains constant. The presence of Si has been only detected in the intermetallic particles. Table IV presents a typical analysis of both second-phase particles and matrix for the sample treated to give the smallest grain size and the material in the as-received condition.

Table IV Chemical composition (EDX) of the second-phase particles and matrix

		Al	Mn	Fe	Cu	Si	Cr	Mn/Fe
condition:	24 mm grain size							
particle	L	63.39	17.31	17.49	1.29	1.35	0.31	0.99
matrix	L	97.82	1.01	0.46	0.71		0.50	2.20
condition:	24 mm grain size							
particle	L	63.39	17.31	17.49	1.29	1.35	0.31	0.99
matrix	L	97.82	1.01	0.46	0.71		0.50	2.20

In order to investigate the characteristics of the distribution of the small particles (≤ 0.1 μm), TEM techniques were employed to analyse samples of the specimens with grain sizes of 320 and 24 μm. The electron micrographs shown in Figures 7 and 8 illustrate the microstructural features observed for both conditions respectively. Thus, a similar small particle distribution has been revealed for both samples constituted by mainly small dispersoids of

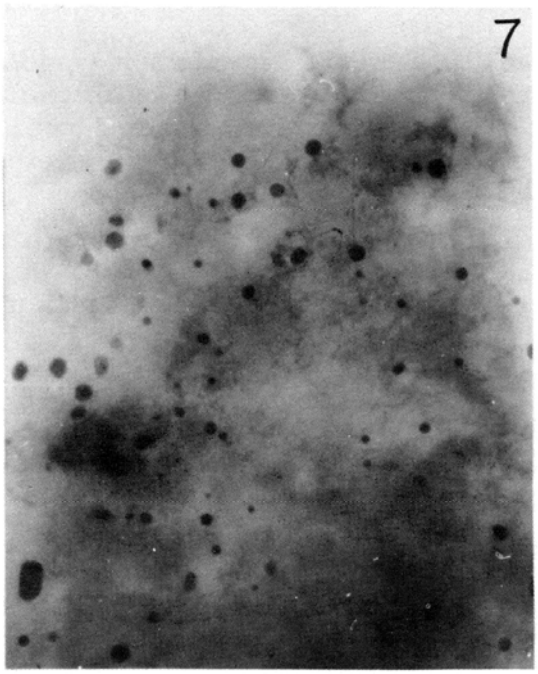

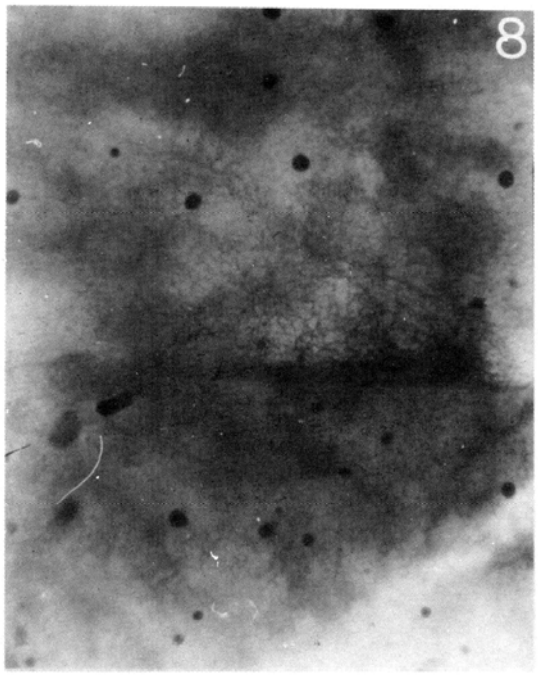

Fig. 7. Transmission electron micrograph showing the distribution of fine second-phase particles present in the 320μm grain size alloy.
Fig. 8. Transmission electron micrograph showing the distribution of fine second-phase particles present in the 24μm grain size alloy.

spherical shape and approximate diameter of 0.5 μm. Such particles have been previously analyzed by other authors [10, 12] and it has been reported that they are mainly composed of Al and Mn with smaller quantities of Si and Fe.

2. Immersion tests

2.1 General Corrosion

Figure 9 illustrates the variation of weight loss as a function of exposure time for different grain sizes, in a solution of NaCl 1M and a pH of 1.5 where a similar behaviour for all the samples is shown. Initially, weight losses are low but increasing with time until a constant value is acheived. The functional dependence encountered is of the type $t^{1/3}$, which agrees with the results obtained by other authors [17-19]. By plotting the variation of the corrosion rate corresponding to the steady state (15 days of exposure), V_C, against the grain size, d, the following linear relationship is obtained:

$$V_C = 0.18 + 3.2 \times 10^{-4}\ d\ (\mu m),\ mg/cm^2.\ day \quad (1)$$

Also, it has been determined that the corrosion rate of the alloy in the as-received condition tested in NaCl 1M is about 0.29 mg/cm^2. day which agrees quite well with the previously reported value of 0.30 mg/cm^2. day, evaluated under similar experimental conditions [10, 11].

2.2 - Pitting corrosion tests

Table V summarize the results obtained from the pitting corrosion tests particularly in relation to the change in the pits depth with the grain size of the material. The reported values in each case, represent the mean value of at least 40 measurements.

Table V Average depth pits

Grain size	(1μm)	24	147	316	320
Depth	(1μm)	18.0	19.3	25.8	30.0

As it can be noticed, there is a slight increase in the pits depth with increasing the grain size. Figure 10 illustrates a scanning micrograph of a transversal section of a pit formed on the surface of the alloy in the as-received condition. However, it should be pointed out that for the exposure times longer than one month the prevailing corrosion is of a general type.

3. Electrochemical tests

3.a - Potentiodynamic tests

Figure 11 illustrates the polarization anodic curves for the alloy in the as-received condition and the samples with different grain sizes. According to the results obtained the behaviour of all tested specimens is quite similar to the previously reported behaviour of pure aluminium [20]. The current density corresponding to the passive zone is displaced towards lower values as the grain size decreases. Such values fluctuate between 0.4 -2.0 $\mu A/cm^2$ in agreement with the previously reported values by Bonewitz [11] of about 0.5 - 2.0 μA/cm2 in sea water using an alloy of similar composition to the one studied in the present investigation. Once again, these results indicate that the material with a smaller grain size presents a better behaviour against corrosion.

However, no marked differences in the values of the pitting potential were found in relation to grain size as it can be observed in Figure 12, although the as-received material presented a more negative potential. The pitting potential for this condition was found to be about -700mV (SCE), which agrees quite well with the value reported by Bonewitz [11] of about -710 mV (ECS), in sea water, and also by Yoshioka [21] of -720 mV (SCE) in NaCl 0.5 N. In the same graphs it has been represented the slight variation of the corrosion potential, determined from the polarization curves with grain size. The values presented are in a good agreement with those determined from immersion tests as it can be observed from table VI.

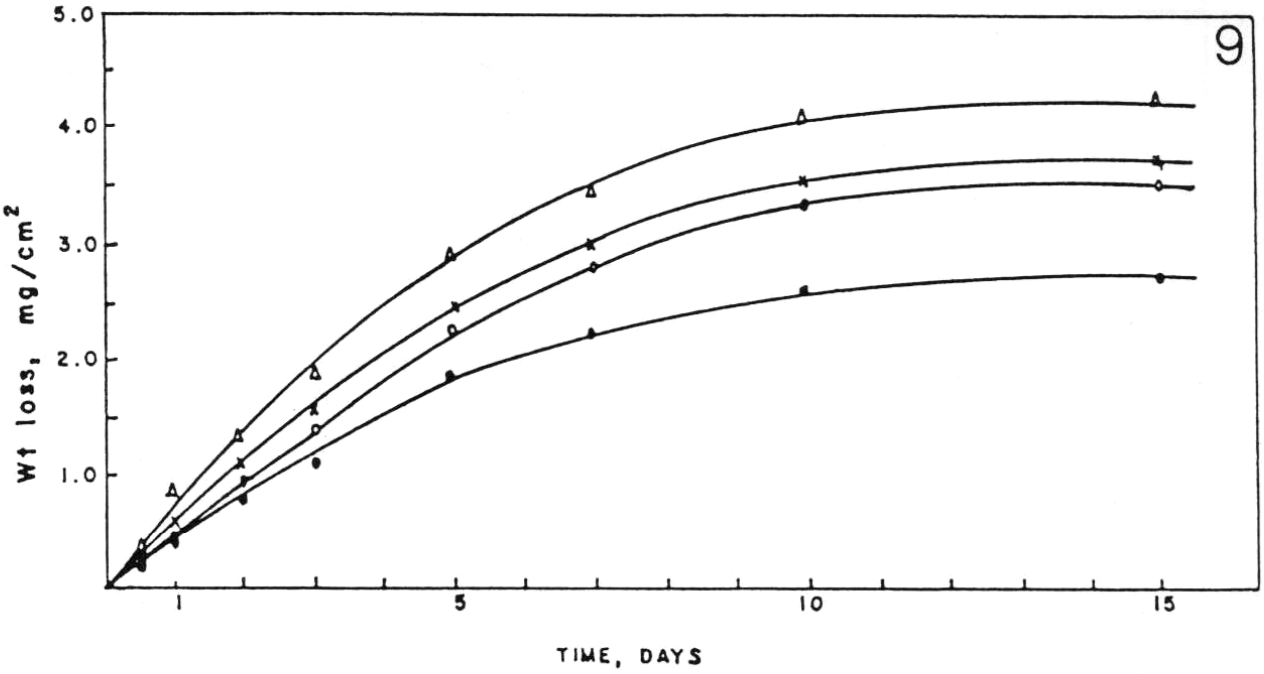

Fig. 9. Weight loss as a function of exposure time for samples with different grain sizes. Solution NaCl 1M, pH=1.5 at 25°C
• 24μm *216μm o 147μmΔ320 μm

Fig. 10. Scanning electron micrograph showing a cross sectional view of a corrosion pit formed on the alloy surface. As-recived condition. Solution of Cl^-, CO^-_3, pH=8.

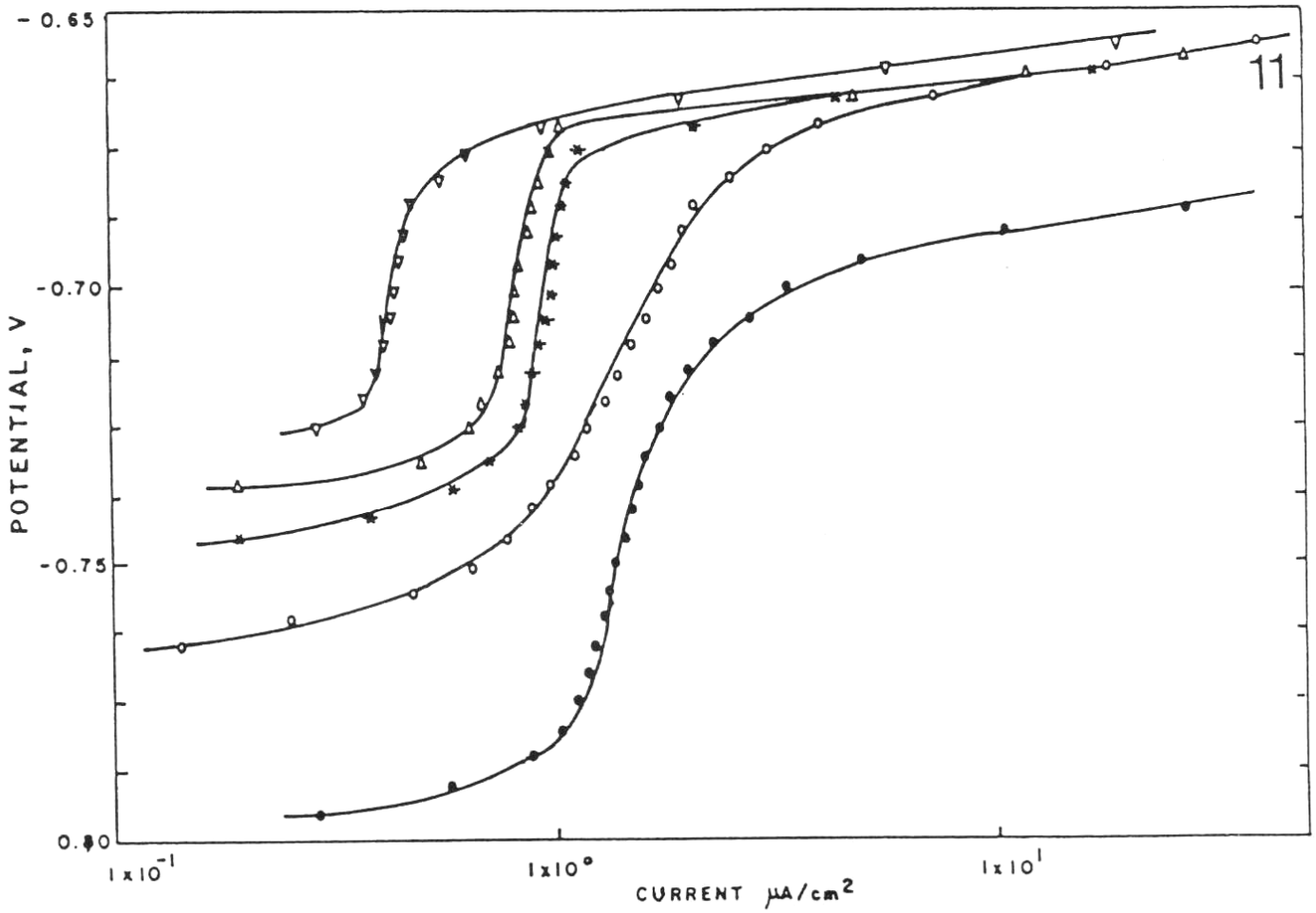
11
- 0.65
-0.70
-0.75
0.80
POTENTIAL, V
1x10⁻¹
1x10°
1x10¹
CURRENT μA/cm²

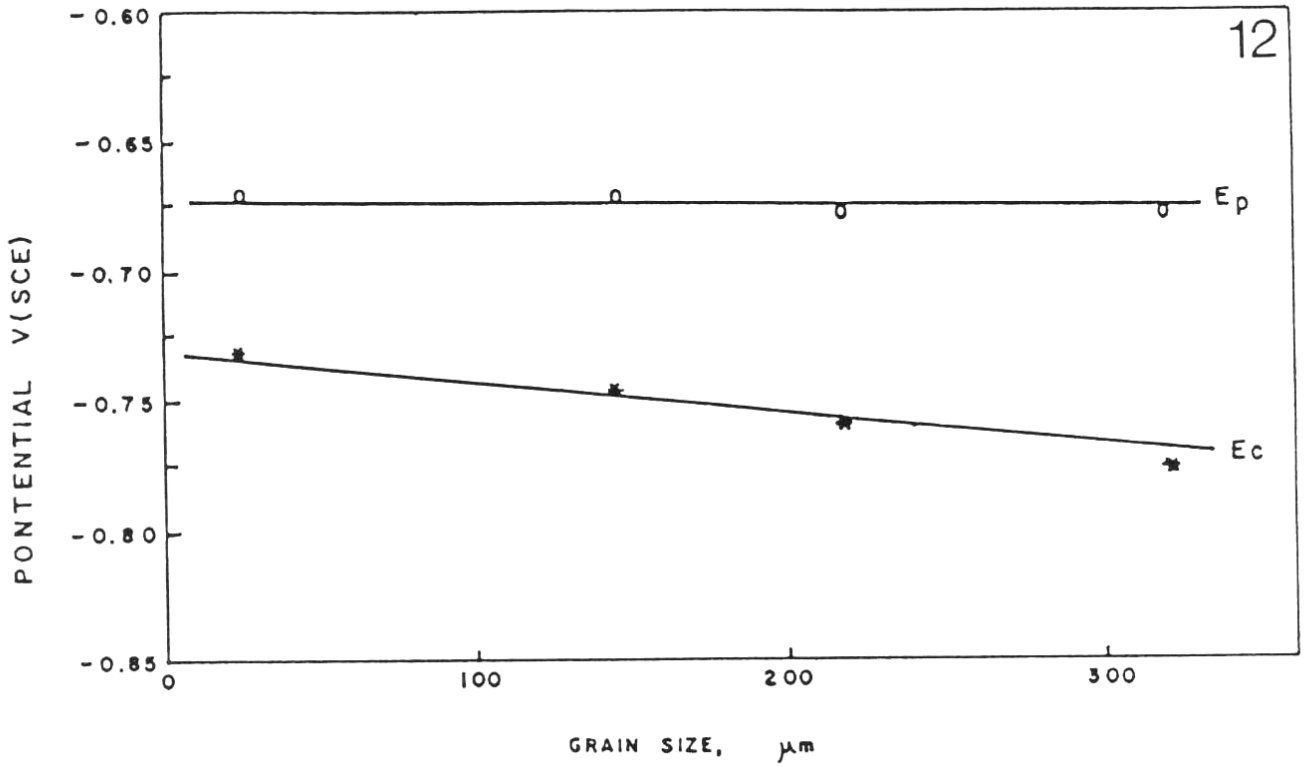
12
- 0.60
- 0.65
-0.70
- 0.75
- 0.80
- 0.85
PONTENTIAL V(SCE)
Ep
Ec
0
100
200
300
GRAIN SIZE, μm

Table VI Corrosion potential determined in samples of different microstructural conditions

d (μm)	24	147	216	320	as-received
E immersion (mV(SCE))	-735	-740	-745	-750	-770
E polarization (mV(SCE))	-730	-745	-755	-770	-800

3.b - Potentiostatic tests

In order to determine the influence of grain size on the current density, a number of tests at constant potential between 5 and 10mV above the pitting potential were carried out. Figure 13 illustrates the curves of current density as a function of time. As it can be observed, during the first stage there is an increase of the current density with grain size, the former ranging between 4-16μA/cm^2. However, the current density tends to achieve a steady state due to the formation of the corrosion products (Al (OH)$_3$, Al_2O_3. $3H_2O_2$, $AlCl_3$) that build up within the pits. The determined current density values corresponding to steady state were of 9, 11, 15 and 22 μA/cm^2 for grain sizes of 24, 147, 216 and 320 μm respectively. The sample of the as-received material achieved current density values greater than those observed for the specimens with the largest grain sizes in both stages. Therefore it can be concluded that the grain size has a marked influence both on current density build-up time and on its stabilization.

Scanning electron micrographs corresponding to Figures 14, 15 and 16 illustrate the corrosion attack produced in a sample of the as-received alloy and in the specimens with grain sizes of 320 and 24 μm respectively. Pitting of the commercial aluminium-1% manganese alloy is quite similar to the previously reported behaviour observed in pure aluminium [22], and according to several authors [6], the geometric shapes with clearly defined cristalographic planes would correspond to planes of the type {100}. In the samples corresponding to the thermomechanically treated materials the morphology of the corrosion attack is similar to that observed for the as-received alloy. Once the passive film has been ruptured the attack grows quickly, extending itself to large areas of the metallic surface. However, in some cases the geometric aspect of pitting is hardly observed because of the presence of many corrosion products. Table VII summarizes the results of the analysis of both pits formed and matrix by means of EDX techniques, in the samples previously referred to.

Table VII Elementary analysis pits and matrix for the studied samples

Condition	Location		Elements				
			Mn	Fe	Cu	Cl	Al
as received		pits	3.84	2.98	3.68	0.68	bal
		matrix	2.75	2.09	0.93	---	bal
320 μm grain size	pits	3.00	2.16	2.52	0.59	bal	
		matrix	1.25	1.60	0.95	---	bal
24 μm grain size	pits	6.49	4.54	9.36	0.58	bal	
		matrix	0.91	0.64	0.81	---	bal

In order to study the morphology of the corrosion attack by means of SEM techniques, every sample was subjected to an overpotential of 30 mV above the pitting potential during 30 min.

As it can be appreciated there is an enrichment of Fe and Cu within the pits in relation to the alloy content in the uncorroded matrix. The presence of Cl^- ions has also been

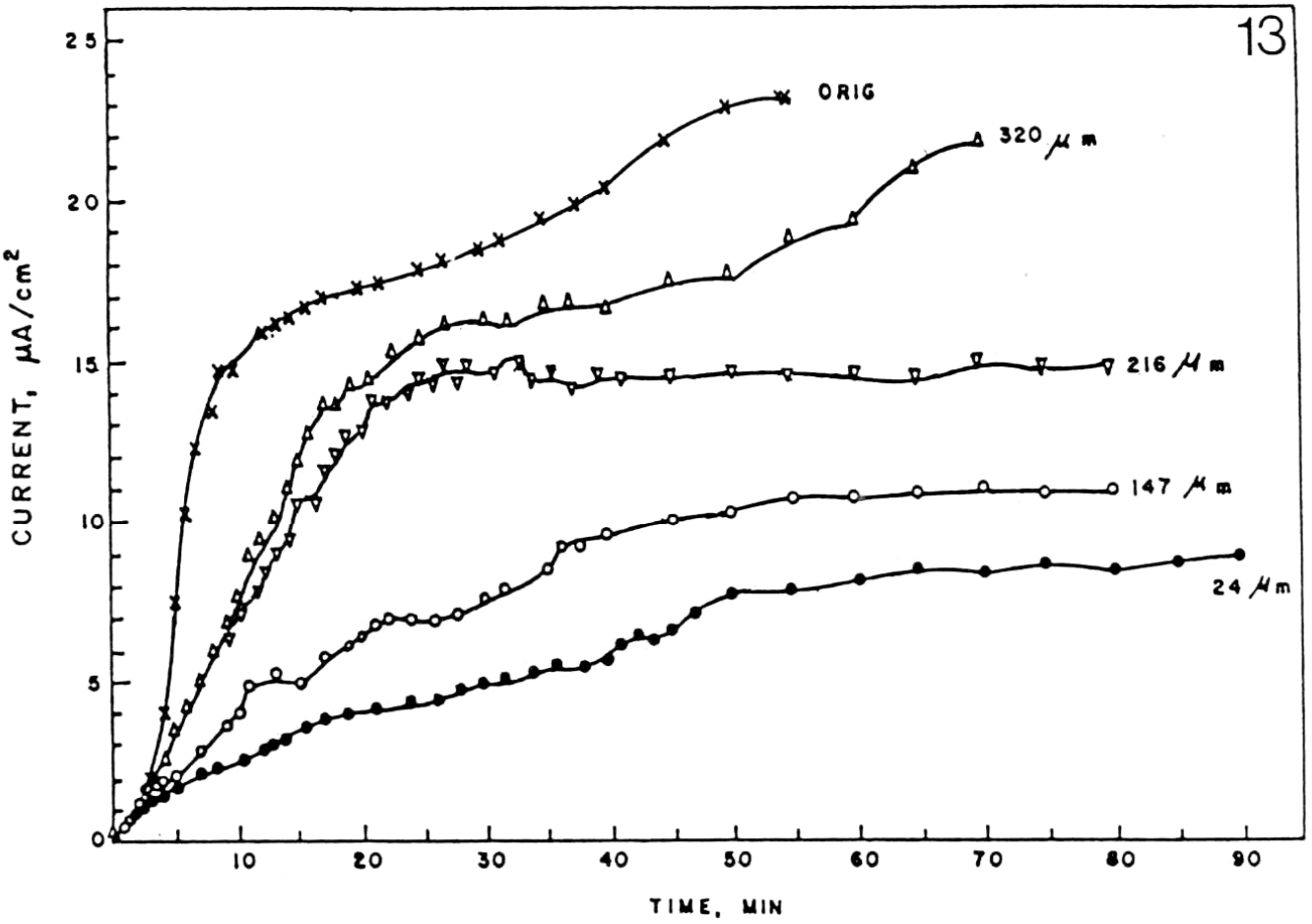

Fig. 11. Polarization anodic curves for the alloy in the as-received condition and thermomechanically treated to produce different grain sizes. Solution NaCl 3.5% at 25ºC.

• as-recived material o 320 μm *216μm
Δ147μm ∇24μm

Fig. 12. Change in the pitting potential (E_p) and the corrosion potential (E_c) with grain size.

Fig. 13. Change in the current density with time for alloy samples in different microstructural conditions at E=-665mV(SCE) in NaCl 3.5% solution purged with nitrogen. T=25ºC

detected, and it was found that the ratio of Fe/Al and Cu/Al were always higher within the pits than in the alloy matrix.

CONCLUSIONS

It has been consistently determined that the corrosion rate of the aluminium-1% manganese alloy decreases as the grain size of the material also decreases. The experiments have shown that the corrosion potential of the alloy is more noble than pure aluminium and that such potential presents a slight displacement towards more positive values as the grain size decreases. On the other hand, from the polarization curves it can be concluded that the corrosion potential are near to those determined from simple immersion tests. Also it was observed that as the grain size decreases a displacement of the current corresponding to the passive zone towards lower values takes place, indicating an improvement of the corrosion behaviour in the agressive medium. In general it has been verified the fact that the investigated alloy exhibits an excellent behaviour against corrosion.

ACKNOWLEDGEMENTS

The authors gratefully acknowledge to the Scientific and Humanistic Research Council (CDCH) of the Central University of Venezuela and to the Organization of the American States (OAS) for the financial support given to the conduction of the present research work.

REFERENCES

[1] Foley, R.T., (1986), "Localized Corrosion of Aluminium Alloys-A Review ", Corrosion,42(5), 277.

[2] Trung H.N. and Foley, R.T., (1979), "On the Mechanism of Pitting of Aluminium", J. Electrochem. Soc. 126 (11), 1855.

[3] Foroulis,Z.A., (1972). "On the significance of the Critical Potential of Pitting of Aluminium in Choloride Solution", Proceedings of the 5th International Congress of Metallic Corrosion, NACE, Tokio, Japan.

[4] Dexter, S.. (1980). "Effects of Oxygen Concentration Variations in the Sea Water upon the Corrosion of Aluminimum Alloys", Corrosion, 36(8), 423.

[5] Ailor, W.H., (1970). "Flowing Sea Water Corrosion Potential of Aluminimum Alloys", Proceedings of 26th Conference of National Asociation of Corrosion Engineers, NACE, USA, 200.

[6] Galvele, J.R. and Muller, I.L., (1977), "Pitting Potential of High Purity Binary Aluminium Alloys. I. Al-Cu Alloys, Pitting and Intergranular Corrosion", Corrosion, 17, 179.

[7] Galvele, J.R. and De Micheli S., (1970), "Mechanism of Intergranular Corrosion of Al-Cu Alloy", Corrosion Science , 10, 795

[8] Leiro, M.C. y Rosales, B (1984), "Factores metalurgicos que controlan la Corrosion por Picado de Aleaciones Aeronáuticas de Al" Latin American Journal of Metallurgy and Materials, 4(1),8.

[9] Lunarska, E. and Szkarspa, S., (1987), "Pitting Corrosion of Powder Metalurgy of Al-Zn-Mn Alloys", Corrosion, 43(4), 219.

[10] Zamin, M., (1981), "The Role of Mn in the Corrosion Behaviour of Aluminium Alloys" Corrosion, 37(11), 627.

[11] Bonewitz, R.A., (1974), "An Electrochemical Evaluation of 3003, 3004 and 5050 Aluminium Alloys for Desalination", Corrosion, 30(2), 53.

[12] Lunder, O. and Nisancioglu, K., (1988), "The effect of Alkaline Etch Pretreatment on the Pitting Corrosion of Wrought Aluminimum", Corrosion, 44(7), 414.

[13] Vera, R., Staia, M.H. and Puchi, E.S., (1992), "Estudios de la Corrosión en la Aleación Commercial de Aluminio -1% Manganeso tratada Termomecánicamente", IVto Congreso Iberoamericano de Corrosión y Protección, Mar de Plata, Argentina.

[14] Modin, H. and Modin, S. (1973), Metallurgical Microscopy, John Willey & Sons, N.Y.

[15] Vera, R., (1990), Tésis M.Sc. en Metalurgia y Ciencia de los Materiales, Universidad Central de Venzuela, Caracas.

[16] Nes, E., (1976), "The Effect of a Fine Particle Dispersion on Heterogeneous Recristalization", Acta Metallurgica, 24, 391.

[17] Gaul, R., (1979), Corrosion of Aluminimum Alloys, Ed. Philip D. Harvey, ASM, Metals Park, Ohio.

[18] Ben Rais, A., Dalard, F. and Sohm, J.C., (1985), "Aluminium Pit Propagation in Acidic Media", Corrosion Science, 25, (11), 1035.

[19] Godard, H.P., (1981), "An Insight into Corrosion Behaviour of Aluminimum", Corrosion, 20 (7), 9.

[20] Beccaria, A.M. and Poggi, G., (1985), "Influence of Hydrostatic Pressure on Pitting of

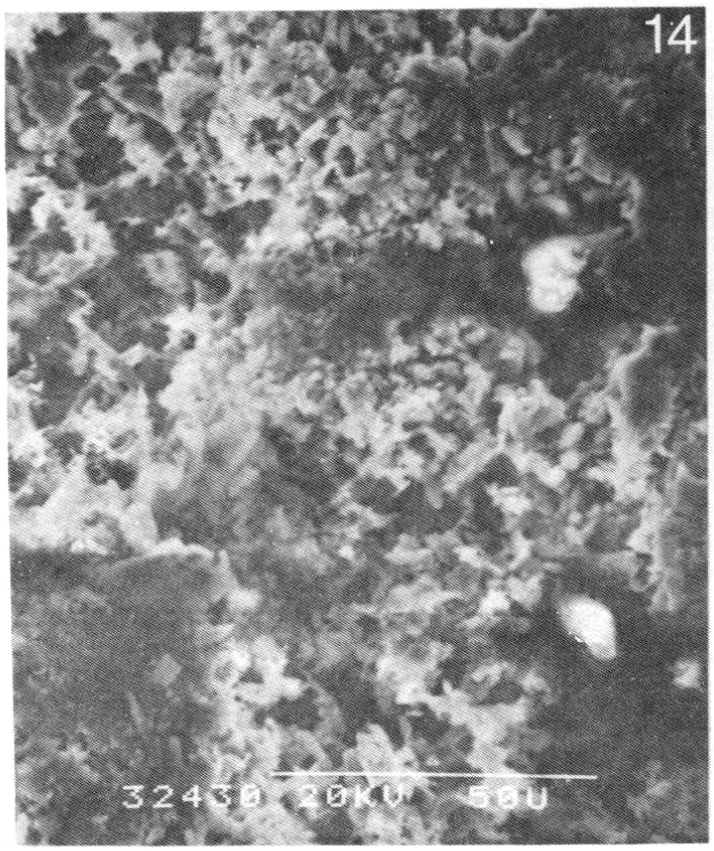

(Continued references)
Aluminium in Sea Water", Br. Corros. J., 20(4), 183.
[21] Yoshioka, H. et al, (1986), "The Pitting Corrosion Behaviour of Rapidly Solified Aluminium Alloys", Corrosion Science 26(10), 813.
[22] Scully, J.C., (1983), Treatise on Materials Science and Technology, vol. 23, "Aqueous Processes and Pasive Films", Academic Press, NY.

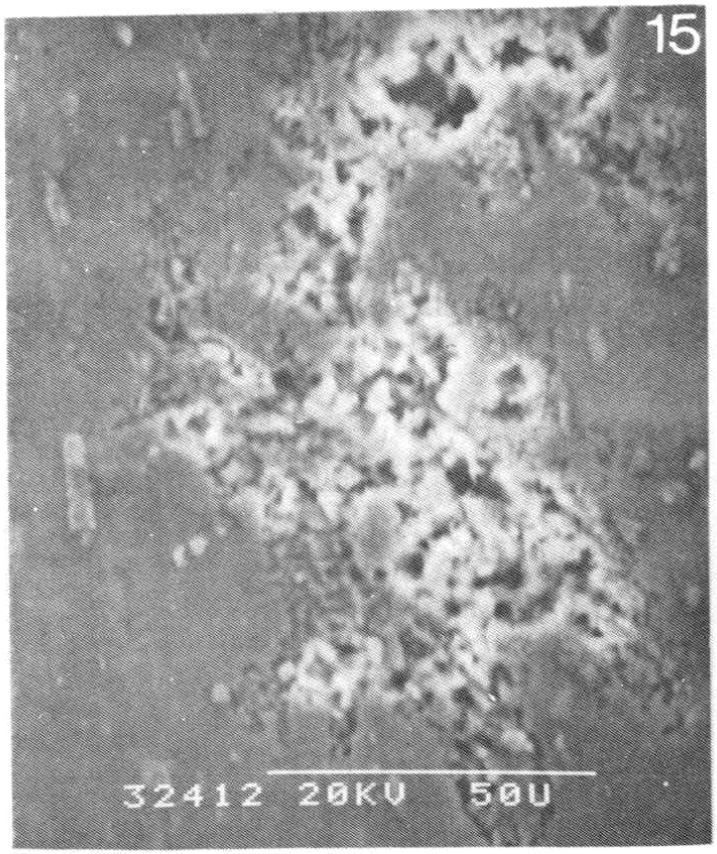

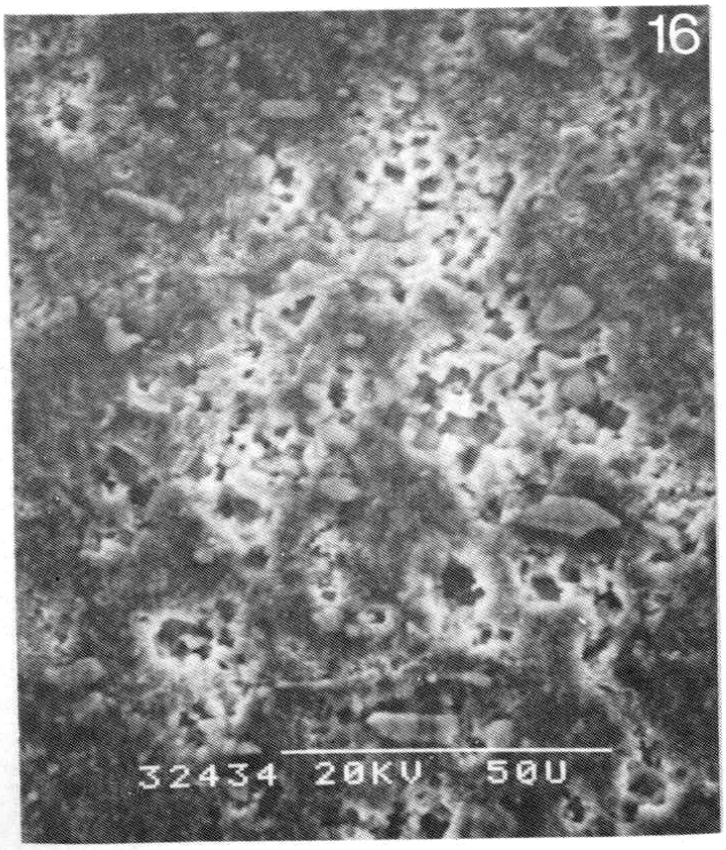

Fig. 14. Scanning electron micrograph showing the corrosion atack produced on the as-recived alloy during the potentiostatic tests.
FIg. 15. Scanning electron micrograph showing the corrosion atack produced on the 320μm grain size alloy during the potentiostatic tests.
Fig. 16. Scanning electron micrograph showing the corrosion atack produced on the 24μm grain size alloy during the potentiostatic tests.